ELSEVIER

Journal of Nuclear Materials 241–243 (1997) 935–940

journal of nuclear materials

Experimental study on highly collisional edge plasmas in W7-AS island divertor configurations

P. Grigull [a,*], D. Hildebrandt [b], F. Sardei [a], Y. Feng [a], G. Herre [a], A. Herrmann [b], J.V. Hofmann [a], J. Kisslinger [a], G. Kuehner [a], H. Niedermeyer [a], R. Schneider [a], H. Verbeek [a], F. Wagner [a], R. Wolf [a], X.D. Zhang [c], W7-AS-Team [a], NBI-Group [a]

[a] *Max-Planck-Institut für Plasmaphysik, EURATOM Ass., Boltzmannstrasse 2, D-85748 Garching, Germany*
[b] *Berlin branch of the IPP Garching, Berlin, Germany*
[c] *Institute of Plasma Physics, Academia Sinica, Hefei, PR China*

Abstract

Edge plasma scenarios in island divertor configurations ('natural' magnetic islands intersected by targets) are studied by comparing data from moderate to high density NBI discharges with 3D code (EMC3/EIRENE) results. The data strongly indicate that high recycling with significant particle flux enhancement was achieved in this geometry. But, plasma pressure losses towards the targets are relatively strong, and high recycling sets in only at $\bar{n}_e > 10^{20}$ m^{-3}. The respective density enhancement in front of the targets is moderate (up to a factor of about three relative to the upstream density). These scenarios are also in basic agreement with B2/EIRENE code predictions. At $\bar{n}_e > 1.5 \times 10^{20}$ m^{-3} detachment seems to develop. Improvements are expected from additional coils controlling the field line pitch inside the islands, and from optimized targets which will better focus recycling neutrals into the islands. Both are in preparation.

Keywords: W7-AS; Helical divertor

1. Introduction

In optimized stellarators it is planned to utilize island divertors, which are based on inherent magnetic islands at the plasma boundary, for proper plasma exhaust. In the present W7-AS stellarator, crucial elements of this concept can be assessed; a full test will be carried out at W7-X. Like stellarators in general, W7-AS is strongly non-axisymmetric, and the edge topology is three-dimensional. The device can be operated with magnetic field configurations bounded by inherent, 'natural' islands of considerable size. The symmetry of the islands is $5/m$ with 5 being the number of magnetic field periods and $m = 7, 8, 9, \ldots$ determined by the respective rotational transform $(\iota/2\pi) = n/m$ [1,2]. The studies on W7-AS had to preclarify to what degree relevant boundary islands are stable with respect to equilibrium currents at finite plasma pressure β, and were subsequently focused on the main questions whether high recycling and related divertor scenarios can be achieved with islands intersected by targets (open arrangement without baffles, see Fig. 1a).

Section 2 describes the edge plasma experiments. In Section 3, the specific edge topology chosen as optimum for this analysis is presented. In that context, results on the island stability at finite β are briefly summarized. This issue is addressed in more detail in Refs. [3,4]. Under these rather complex 3D conditions, the interpretation of local data from the experiments and characterization of respective edge regimes need sophisticated modelling adapted to the special island topology. Section 4 briefly summarizes the present state of code developments (for detailed descriptions see Refs. [5,6]) and describes the adjustment of free input parameters of the utilized code to experimental data. In Section 5, code results are compared with mea-

* Corresponding author. Fax: +49-89 3299 2584; e-mail: grigull@wendelstein.ipp-garching.mpg.de.

PII S0022-3115(96)00635-6

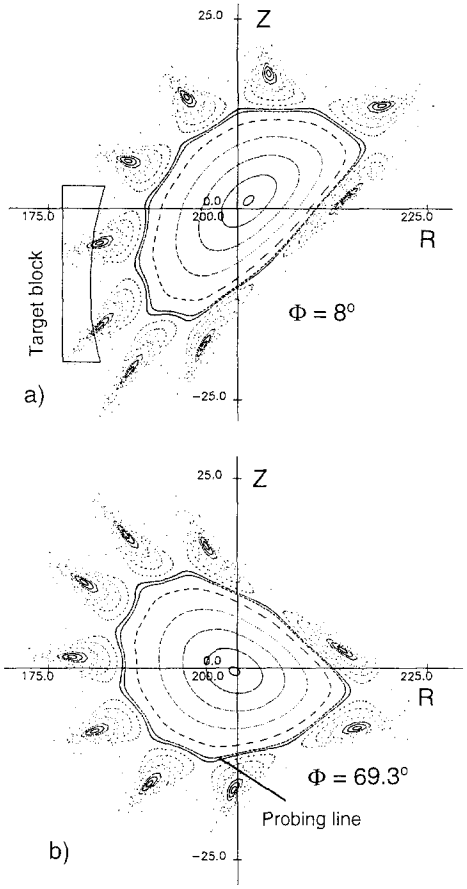

Fig. 1. Cross sections of the W7-AS vacuum magnetic field configuration with 5/9 boundary islands at (a) a target plane and (b) a plane with the FRLP probing line.

sured data, and Section 6 gives a summary on the results and conclusions.

2. Experimental

The analysis was made for net current compensated NBI discharges at $B = 2.5$ T with ECRH start-up and balanced injection. Line-averaged densities $\bar{n}_e$ were varied between 2×10^{19} and 1.5×10^{20} m^{-3}. Heating powers were 0.8 MW for $\bar{n}_e \leq 8 \times 10^{19}$ m^{-3} and 2 MW for higher densities. Data were taken during flat-top phases of about 300 ms (low to moderate densities) or 150–200 ms (highest densities). In the latter case, density control was lost in general after that time and the discharges were radiatively terminated before switching off the heating power. The edge rotational transform $\iota_a/2\pi$ was 0.564 which corresponds to a configuration with 5/9 boundary islands. Edge plasma parameters were obtained from two Langmuir probes (CFC tips): a fast reciprocating probe (FRLP) at the position shown in Fig. 1b, and a second probe close to a target. Both probes were operated in the single mode; n_e and T_e values were derived by fitting the probe characteristics up to the floating potential [7]. The measurements were completed by Thomson scattering, spectroscopic observation (H_α diode arrays looking at the targets, CCD cameras with filters for H_α or CIII radiation), bolometry, low-energy CX neutral analysis (LENA) and target thermography.

3. Edge topology

Magnetic field configurations with $5/m$ boundary islands calculated by the KW equilibrium code [8] show, up to $\beta_0 \approx 1\%$, increasing island radial elongations and field line pitch, but intact island surfaces and preserved symmetry. This is in good agreement with experimental signatures from probe measurements, camera observations and thermographic patterns at the targets [3,4] and holds, in particular, also for the configuration with $\iota_a/2\pi = 0.564$ (5/9 islands) which was chosen as optimum for the present analysis. At $B = 2.5$ T, the β_0 range up to about 1% essentially covers the accessible discharge regimes studied. The 5/9 configuration offers both, sufficient main plasma cross section and relatively large boundary islands (Fig. 1a, b). Typical island dimensions in the radial and poloidal directions are 5–10 cm (depending on the helical position). Field line connection lengths L_c between stagnation points and targets for the probing line and relative probing positions x/L_c (with x being the parallel distance from the stagnation point) are shown in Fig. 2. As can be seen, moving along the probing line across the island does not only alter the perpendicular distance from the island separatrix, but also strongly L_c and x/L_c. At higher β, L_c

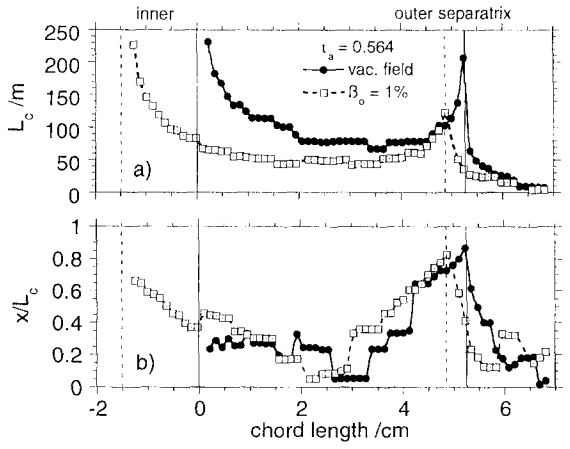

Fig. 2. (a) Field line connection lengths L_c between stagnation point and target as seen by the FRLP, and (b) relative, parallel distances x/L_c of the probe from stagnation point for the vacuum magnetic field and at $\beta_0 = 1\%$. Positions of the island separatrix are indicated.

becomes smaller (increased field line pitch, as mentioned above) and the island separatrix is shifted inwards, at the radial inside stronger than at the outside.

The target setup consists of ten poloidal graphite blocks (CFC) with toroidal widths of 12 cm, two per magnetic field period (one of them is shown in Fig. 1, the second, covering the upper half of the radial inside, is at an equivalent, mirror-symmetric position). Effectively, they cover the inboard side of the plasma close to the toroidal midplane of each field period.

4. Modelling approaches

The edge plasma was modelled for the 5/9 island topology by a 2D (B2, time-resolving, multi-fluid [6,9,10]) and a 3D approach (EMC3 [5]), each coupled with the EIRENE neutral transport code [11,12]. The B2 approach allows to study basic divertor properties with sophisticated physics, but includes helical averaging of the island configuration and can in particular not treat the present target geometry and hence the interaction with neutrals in a fully realistic way. Furthermore, it does not allow direct reference to local experimental data in the actual 3D configuration. The EMC3 code solves the set of fluid equations by a Monte Carlo technique considering the full non-axisymmetric geometry, but includes at present some physics simplifications: it treats single fluid plasma only, neglects heat convection and treats volumetric momentum losses by parametrization (see below). This is not caused by basic problems of the code, and an extension to more complete physics is under way. At present, we restrict ourselves to a 'complementary' description: the EMC3 code input parameters are adjusted to match local, experimental data, and the tendencies derived from this are then compared with B2/EIRENE predictions by brief reference in Section 6.

The basic equations solved by the EMC3 code [5] are

$$\nabla\cdot\left(n\vec{v}_{\parallel}-D_{\perp}\nabla_{\perp}n\right)=S_{\mathrm{p}}, \tag{1}$$

$$\nabla_{\parallel}\left(m_{\mathrm{i}}nv_{\parallel}^{2}+p\right)=-\alpha, \tag{2}$$

$$\nabla\cdot\left(-\kappa_{\parallel}\nabla_{\parallel}T-\chi_{\perp}n\nabla_{\perp}T\right)=S_{\mathrm{e}} \tag{3}$$

with $n_{\mathrm{e}}=n_{\mathrm{i}}=n$, $T_{\mathrm{i}}=T_{\mathrm{e}}=T$, $p=2nT$, $\kappa_{\parallel}\propto T^{5/2}$ and the boundary conditions at the target $\Gamma_{\mathrm{t}}=n_{\mathrm{t}}c_{\mathrm{st}}$, $q_{\parallel\mathrm{t}}=\Gamma_{\mathrm{t}}\gamma T_{\mathrm{t}}$. n_{e}, n_{i} are the electron and ion desities, $v_{\parallel}$ is the parallel ion velocity, m_{i} the ion mass, $D_{\perp}$ and $\chi_{\perp}$ are the cross field particle diffusion coefficient and electron heat diffusivity, T_{e} and T_{i} the electron and ion temperature, S_{p} and S_{e} are volumetric particle and energy sources or sinks, the parameter α denotes momentum sinks, Γ is the particle flux and c_{s} the ion sound speed. S_{e} considers only energy losses due to neutral hydrogen. The energy transmission factor γ was set to eight [7].

The code has five free input parameters: $D_{\perp}$, $\chi_{\perp}$, α, the power flow P_{s} across the inner separatrix and the density n_{es} at the inner separatrix. P_{s} was estimated from the deposited part of the NBI power and the total power radiated from the core (from bolometer data), $P_{\mathrm{s}}=P_{\mathrm{NBI,dep}}-P_{\mathrm{rad,core}}$. In agreement with the density dependent relation of $\chi_{\perp}/D_{\perp}$ as observed in W7-AS at $\iota/2\pi=0.34$, $\chi_{\perp}$ was set to $3\times D_{\perp}$. The remaining free quantities n_{es}, $D_{\perp}$ and α were obtained by adjusting them to match

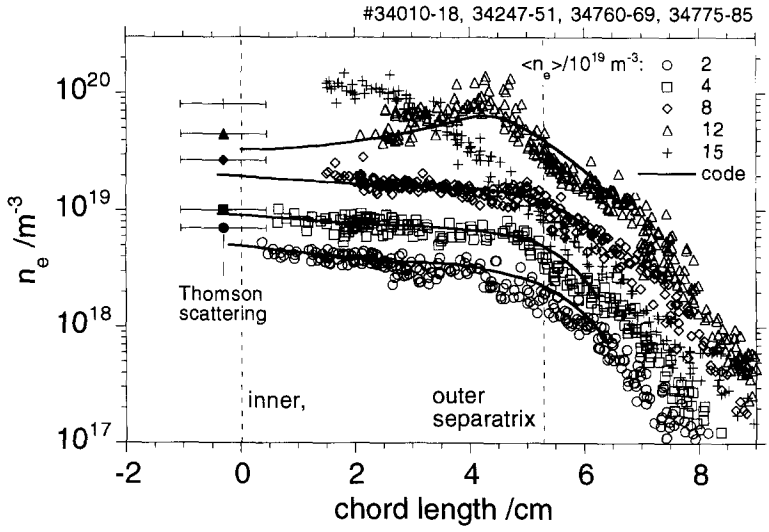

Fig. 3. Electron density profiles measured by the FRLP across an island, Thomson scattering data measured close to the inner separatrix, and EMC3/EIRENE simulations of the probe data. Positions of the island vacuum field separatrix are indicated. In the discharges with high density and NBI power (see text), $\beta_0\approx 1\%$ is achieved which means that the actual separatrix positions are slightly shifted inwards. Code input data were adjusted to match the probe data at the innermost probe positions, at the outermost calculated points, and at a further probe position close to a target (see Fig. 5).

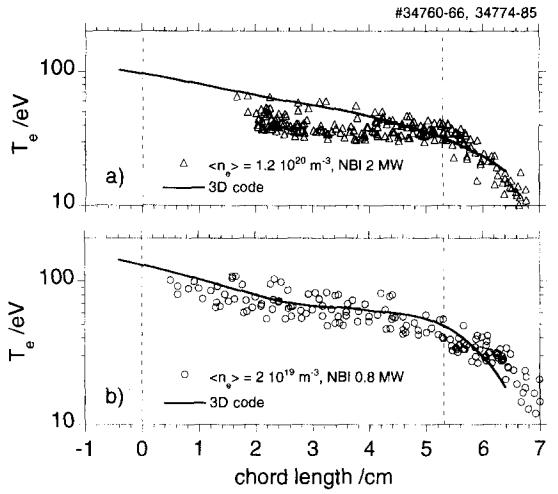

Fig. 4. Electron temperatures T_e from the FRLP and respective EMC3/EIRENE simulations at (a) high and (b) low line-averaged density.

experimental densities from Langmuir probes at three points: at the position closest to the inner separatrix accessible by the FRLP without disturbing the core plasma (upstream position), a respective point within the private sector (see density profiles in Fig. 3), and at the position of the second probe in the proximity of one of the targets ($x/L_c = 0.97$).

5. Results and discussion

Fig. 3 shows n_e profiles across an island measured by the FRLP, and respective EMC3/EIRENE results. As can be seen, the measured profiles are, up to moderate line-averaged densities, rather flat inside the island and show a pronounced maximum close to the outer separatrix ('divertor tail') at $\bar{n}_e = 1.2 \times 10^{20}$ m^{-3}. At the highest density, the maximum of the profile is shifted inwards indicating (at least partial) detachment. This latter interpretation is supported by camera observations of the H_α and CIII lines from the targets. The H_α stripes along the strike points (radial observation) vanish, the radiation becomes diffuse and much weaker. At the same time the CIII radiation (tangential view) becomes concentrated at the X-point proximity, and the integral power onto the targets is decreased to below 10% of the heating power (from thermography). Parallel with increasing density (loss of density control, Section 2) the hot plasma cross section shrinks, and the discharges become terminated. The density profiles up to $\bar{n}_e = 1.2 \times 10^{20}$ m^{-3} are quite well reproduced by the code (modelling of detached scenarios would not be reasonable with the present EMC3 version). Particle diffusion coefficients resulting from the code adaption are $D_\perp = 0.6$ m^2/s for $\bar{n}_e \leq 8 \times 10^{19}$ m^{-3} and 0.2 m^2/s for $\bar{n}_e = 1.2 \times 10^{20}$ m^{-3}. The values of $D_\perp$ do, within factors of about 2, not critically affect the calculated profiles within the island, but are rather sensitive in reproducing the steep density drop towards the private sector. They are significantly smaller than derived for configurations with non-resonant boundary [13] and may indicate changed transport in island configurations, at least in the private sector. As is shown in Fig. 4, the measured T_e profiles are satisfactorily reproduced by the code only at low density. The discrepancy at higher density indicates stronger radiative losses due to impurities (mainly carbon) not considered by the code.

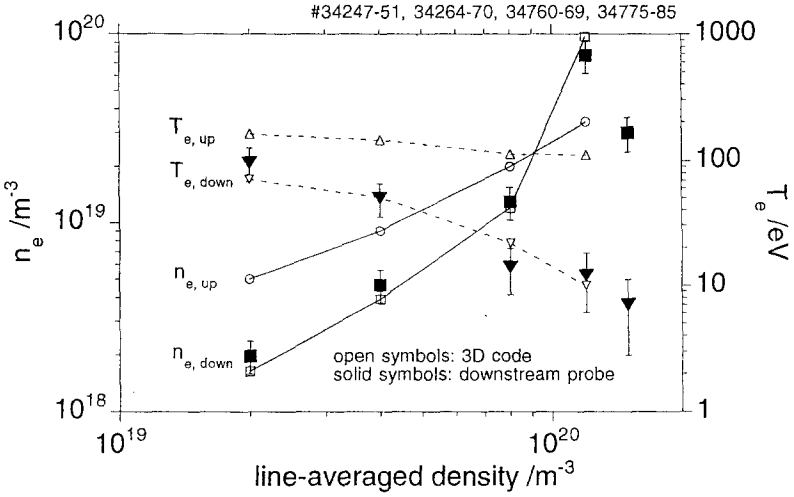

Fig. 5. Upstream and downstream n_e and T_e values (averaged along the strike line) from the EMC3/EIRENE code and data from the downstream probe versus the line-averaged density for the discharge series shown in Figs. 3 and 4. Error bars indicate statistical errors, lines are for guiding the eyes only. Local downstream densities from the code were matched to the probe data.

In Figs. 5 and 6, respective upstream and downstream data from the experiments and the code are plotted versus the line-averaged density. As can be seen, the downstream density increases up to a value of about three times the upstream density at $\bar{n}_e = 1.2 \times 10^{20}$ m^{-3}, whereas the downstream T_e drops to about 10 eV. Energy losses due to neutral hydrogen reach up to about 50% of the power flow across the main plasma separatrix. Relative H_α intensities from the target show a similar tendency as the downstream densities and are well reproduced by the code. At high density, the scrape-off layer (SOL) becomes opaque for neutrals, and the total particle efflux from the SOL relative to that across the main plasma separatrix reaches up to a factor of about 35. Energy spectra of escaping CX neutrals from LENA (not shown) indicate, up to $\bar{n}_e = 8 \times 10^{19}$ m^{-3}, a linear decrease of the mean energy with increasing $\bar{n}_e$, but switch rather abruptly to much smaller mean energy at $\bar{n}_e = 1.2 \times 10^{20}$ m^{-3}. These are clear signatures for a high recycling scenario as it is known from tokamak divertors [7,14]. At the highest density, the measured downstream density and H_α intensity show 'roll over' indicating detachment as mentioned above. The present EMC3 version does not yet allow a quantitative appointment, but momentum transfer by charge exchange neutrals is, as in tokamak divertors, expected to be crucial for the transition from high recycling to detachment. Nevertheless, the data indicate strong plasma pressure losses along the island fans also in the attached regimes at low to moderate density which, in effect, shift the onset of high recycling to very high density and limit the respective density enhancement in front of the targets to moderate values. Though not fully comparable, B2/EIRENE results [6] show, at low to medium recycling, similarly excessive pressure parallel drops within the power carrying layer which are mainly balanced by the radial convective momentum flux and viscosity terms.

6. Summary and conclusions

The SOL of moderate to high density NBI discharges in a magnetic field configuration with 'natural' boundary islands intersected by targets was analyzed with respect to divertor scenarios. Experimental data and EMC3/EIRENE code results strongly indicate that, different from limiter scenarios, a concentration of the particle sources inside the SOL and significant particle flux enhancement were achieved. But relatively strong plasma pressure drops towards the targets indicating considerable volumetric momentum losses restrict 'classical' divertor high recycling scenarios to very high density ($\bar{n}_e \geq 10^{20}$ m^{-3}, $n_{es} \geq 3 \times 10^{19}$ m^{-3}) and limit the respective density enhancement in front of the targets to factors of about three relative to the upstream density. Quite similar scenarios are predicted by B2/EIRENE calculations [6] for the helically averaged island geometry and otherwise equivalent conditions, but high recycling sets already in at $n_{es} > 10^{19}$ m^{-3} which is primarily appointed to the deviating target geometry in the 2D treatment. At $\bar{n}_e \geq 1.5 \times 10^{20}$ m^{-3} the experimental data indicate detachment, but do not yet allow statements on the stability behavior of this scenario. Further experiments on this issue at conditions with improved density control (NBI combined with 140 GHz ECRH), together with a code analysis considering also detailed momentum balance and light impurity radiation, are under way.

An extension of the density range with divertor high recycling and improved conditions for the establishment of stable detachment are expected from additional coils con-

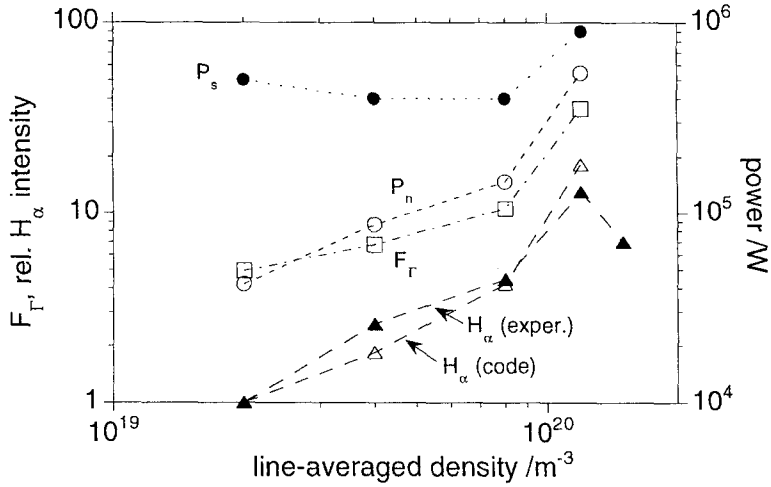

Fig. 6. Power flow P_s across the main plasma separatrix (input for the EMC3/EIRENE code, see text), total volumetric power losses P_n due to neutral hydrogen, and particle flux enhancement factors F_Γ from the code versus the line averaged density. Relative H_α intensities from the target and respective values reproduced by the code (both normalized to unity at the lowest density).

trolling the field line pitch inside the islands, and from helically more extended, optimized targets [3]. The latter will better approximate to 2D conditions and allow, in particular, improved focusing of recycling neutrals into the islands. Both additions are in preparation.

References

[1] R. Jaenicke et al., Nucl. Fusion 33 (1993) 687.
[2] P. Grigull et al., J. Nucl. Mater. 196–198 (1992) 101.
[3] F. Sardei et al., these Proceedings, p. 135.
[4] J.V. Hofmann et al., 10th Intern. Conf. on Stellarators, IAEA Technical Meeting, Madrid, Spain, 1995, Report EUR-CIEMAT, Vol. 30 (1995) p. 77.
[5] Y. Feng et al., these Proceedings, p. 930.
[6] G. Herre et al., these Proceedings, p. 941.
[7] P.C. Stangeby et al., Nucl. Fusion 30 (1990) 1225.
[8] J. Kisslinger and H. Wobig, 12th European Conf. on Controlled Fusion and Plasma Physics, Budapest, Hungary, 1985, Europhys. Conf. Abstr. 9F, 1, p. 453.
[9] B.J. Braams, Report (NET) EUR-FU/XII-80/87/68, Comm. of the EC, Brussels, 1987.
[10] R. Schneider et al., J. Nucl. Mater. 196–198 (1992) 810.
[11] D. Reiter, J. Nucl. Mater. 196–198 (1992) 80.
[12] D. Reiter, J. Nucl. Mater. 220–222 (1995) 987.
[13] P. Grigull et al., 10th Intern. Conf. on Stellarators, IAEA Technical Meeting, Madrid, Spain, 1995, Report EUR-CIEMAT, Vol. 30 (1995) p. 73.
[14] A. Loarte, these Proceedings, p. 118.